MATERIALS CHEMISTRY
FRONTIERS

CCS 中国化学会 CHINESE CHEMICAL SOCIETY
ICCAS
ROYAL SOCIETY OF CHEMISTRY

RESEARCH ARTICLE

View Article Online
View Journal | View Issue

Cite this: *Mater. Chem. Front.*, 2022, **6**, 765

A novel eco-friendly strategy on the interfacial modification of a carbon-fiber-reinforced polymer composite *via* chitosan encapsulation†

Cheng Zhang,[a] Xueqin Zhang,[a] Youquan Ling,[a] Tong Sun,[a] Mei Liang,[a] Zhengguang Heng,*[a] Huawei Zou,*[a] Zhong Zeng[b] and Hui Liu[b]

Received 7th December 2021,
Accepted 24th January 2022

DOI: 10.1039/d1qm01587g

rsc.li/frontiers-materials

The interfacial properties are the key factors that affect the properties of carbon-fiber-reinforced polymer (CFRP) composites. Therefore, it is necessary to modify the surface of CF. However, most of the methods face problems of complex technology and environmental pollution. Here, the biomass material chitosan (CS) was encapsulated on the surface of the CF using a one-step method. The surface roughness and wettability of the CFs were improved markedly. When the content of CS was 0.05 wt%, a uniform membrane structure with a thickness of 32 nm was formed. Furthermore, the CS-encapsulated CFRP composites were prepared from the optimal multilayer structure. Compared with untreated CFRP composites, the interfacial shear strength, transverse fiber bundle test tensile strength, and interlaminar shear strength of the CS-encapsulated CFRPs increased by 53.65%, 34.15%, and 15.67%, respectively. This modification method is simple, eco-friendly, and non-destructive. It provides a new way to expand the application of CS in the field of CFRP composites.

1 Introduction

Carbon-fiber-reinforced polymer (CFRP) composites are widely used in aviation, the military, industry, construction, sports, and leisure products, profiting from their high strength, lightweight properties, and good environmental stability.[1–4] With the performance requirements of CFRP composite materials increasing, high-strength and high-modulus CFs have been widely used.[5] However, composites reinforced with untreated CFs show a poor fiber matrix interaction due to the chemical inertness and smoothness of the CF surface. This poor interaction affects the overall performance of the composite material; thus, the interface layer between the CF and the matrix plays a key role in the performance of composite materials.[6,7] The perfect interface can eliminate the concentration of stress and transfer the load from the matrix to the fiber.[8] Therefore, a good interface structure is conducive to improving the properties of CFRP composites.

In recent years, numerous methods have been used to improve interface performance. Fu *et al.*[9] performed anodization activation by electrochemically oxidizing the surface of high-modulus CF, and then grafted diethylene triamine *via* electrochemical grafting. Sun *et al.*[10] built a multi-scale structure to improve the interface strength of epoxy resin composites through electrophoretic deposition and electropolymerization of the CF surfaces. The electrochemical method can greatly improve the surface roughness and specific surface area of the CF, although it may damage it a little.[11] Montes-Morán *et al.*[12] studied the effect of plasma treatment on the interface properties of CF–thermoplastic composites. Plasma changed the microstructure of the fiber through etching, destroying its body performance. In addition, the plasma causes a certain degree of damage to the operator. Yao *et al.* improved the roughness of the fiber by functionalizing the growth of carbon nanotubes on the CF fabric through chemical vapor deposition (CVD).[13,14] However, CVD can introduce metal ions and cause serious damage to the fiber.[15] Wu *et al.* used a polydopamine (PDA)-based carbon coating to grow carbon nanotubes on CFs using the CVD method. It effectively mitigates the corrosion of the fiber caused by the high temperature and the metal catalyst in the CVD process, thereby improving the mechanical properties of the composite material.[16] Ma *et al.* proposed a method to improve the interfacial adhesion between TiO_2 nanoparticles and CFs using the functionalization of amine groups in supercritical water.[17] Peng *et al.* used polyamidoamine to functionalize CFs.[8,18] Ma *et al.* used polyethyleneimine as a coupling agent to functionalize CFs through both conventional and supercritical processes.[19] Improving the

[a] *The State Key Lab of Polymer Materials Engineering, Polymer Research Institute of Sichuan University, Chengdu 610065, China. E-mail: hengzhengguang@163.com, hwzou@163.com*
[b] *Safety Environment Quality Surveillance and Inspection Research, Institute of CNPC Chuanqing Drilling & Exploration Corporation, Chengdu 618300, China*

† Electronic supplementary information (ESI) available. See DOI: 10.1039/d1qm01587g

wettability, connecting rod mechanism, and chemical interactions to improve the interfacial properties of the CFs has been proved to be an effective strategy.[17] However, nano-particles or single macromolecules are only attached to the surface of the fiber through simple mechanical interlocking and physical interactions and have little effect on the interface.[20] Chu *et al.* studied the sizing of the carbon dot bridging sizing agent on the surface of the CFs to improve the interface between the fiber and resin.[21] Wu *et al.* used polydopamine (PDA) to modify the interface of CFs to prepare high-performance composite materials with a designable interface bonding strength. After annealing, the interlaminar shear strength (ILSS) value of the composite material increased by 38.73% and the retention rate reached 92.61%.[22] Sizing makes the interface more uniform, and the surface of the CFs has good interface properties. However, the sizing agent was expensive and not environmentally friendly. It is necessary to choose an eco-friendly and non-destructive method to improve the interface performance.

Chitosan (CS) has the advantages of being widely available, non-toxic, degradable, having good biocompatibility, showing strong biodiversity, is easy to form a membrane, *etc.*[23,24] CS can be chemically modified *via* crosslinking, grafting, acylation, and etherification, because it contains a large amount of $-NH_2$ and –OH groups.[25] Tang *et al.*[26] prepared an antibacterial material by loading AgNPs on the surface of activated CFs with CS. The results have shown that CS was a promising binder. The surface modification of silk fibers with anhydride-grafted CS and the dyeing properties of grafted silk were studied by Davarpanah *et al.*[27] The mechanism of CS-modified degummed silk *via* acid anhydride grafting was put forward. The preparation of CS/lignosulfonate multilayer membranes on the fiber surface using a layer-by-layer deposition technique was studied.[28] The formation of CS/lignosulfonate multilayers on the surface of cellulose fibers was confirmed. The above research provides a theoretical basis for the application of CS.

In our work, commercial CFs were desized (DCFs) and oxidized (OCFs), and CS was encapsulated on OCFs (OCFs-CS) using a sizing procedure. Then, CFRP composites were prepared by impregnating the OCFs-CS with epoxy resin. The microstructure and micromorphology of the OCFs-CS were confirmed *via* Raman, X-ray photoelectron spectroscopy (XPS), Fourier transform infrared spectroscopy (FT-IR), scanning electron microscopy (SEM), transmission electron microscopy (TEM), and contact angle measurements. The effect of the CS concentration on the interlaminar behavior of the final composites was thoroughly discussed in terms of the interfacial shearing strength (IFSS), transverse fiber bundles test (TFBT) tensile strength, and the ILSS method.

2 Experimental

2.1 Materials

The materials and suppliers used in this study are shown in Table 1. The structural formula of the epoxy resin and curing agent in this study are presented in Fig. S1 (ESI†).

2.2 CS-encapsulated CFs

First, the CFs were desized in acetone solvent at 363.15 K for 60 h. After washing with deionized water five times, the DCFs were dried overnight at 353.15 K under vacuum. Second, the DCFs were oxidized in a solution of $AgNO_3$ (0.01 mol L^{-1})/$K_2S_2O_8$ (0.1 mol L^{-1}) at 343.15 K for 1 h.[29] Third, CS (0.025, 0.05, 0.075, and 0.1 wt%) was dissolved in acetic acid solution (3 mol L^{-1}) and thoroughly mixed under ultrasound. OCFs were dipped in the above-mentioned solution for 5 min for sizing. The OCFs after CS encapsulation were designated as OCFs-CS1, OCFs-CS2, OCFs-CS3 and OCFs-CS4. The reaction flow diagram is shown in Fig. 1a.

2.3 Preparation of CFRP composites

The schematic figure of CFRP composite preparation is shown in Fig. 1b. The optical pictures for sizing and fabricating the unidirectional CFRP composites are provided in Fig. S2 (ESI†). The fibers were fully dispersed and wound on cardboard, and then the fibers were impregnated with epoxy resin. After the epoxy resin had fully infiltrated the fibers, the infiltrated fibers were then laid flat in a mold. The composite was fabricated using a custom-made mold (2 mm in thickness and 6 mm in width). The volume fraction of CFs in the composite was 60 ± 1.5%. TDE-85, DDM, and DETDA were combined in the ratio of 10 : 7 : 3. The composite molding conditions were based on our previous research work (353.15 K for 1 h and 393.15 K for 2 h at 5 MPa pressure, 423.15 K for 3 h and 453.15 K for 1 h at 10 MPa pressure).[30]

2.4 Characterization

The surface structure of the CFs was measured using Raman spectroscopy (Dilor, France). The surface elemental change of the fibers was analyzed using XPS (PHI5000 Versaprobe-II, Japan). The chemical structure of the fibers was analyzed *via* FT-IR (Nicolet 570, USA) scanning the wavenumber range from 4000 to 400 cm^{-1}.

Table 1 Materials used in this study

Material	Supplier
CF (T700)	Toray Industries, Inc., Japan
$K_2S_2O_8$, $AgNO_3$, CS	Shanghai Aladdin Industrial Co. Ltd., China
Acetic acid	Tianjin Bodi Chemical Co. Ltd., China
4,5-Epoxycyclohexane-1,2-dicarboxylic acid diglycidyl ester epoxy resin (TDE-85)	Shanghai Jixi Trade Co., Ltd., China
4,4-Diamino diphenyl methane (DDM)	Shanghai Acmec Biochemical Co. Ltd., China
Diethyltoluenediamine (DETDA)	Shandong Fanhang Chemical Co. Ltd., China

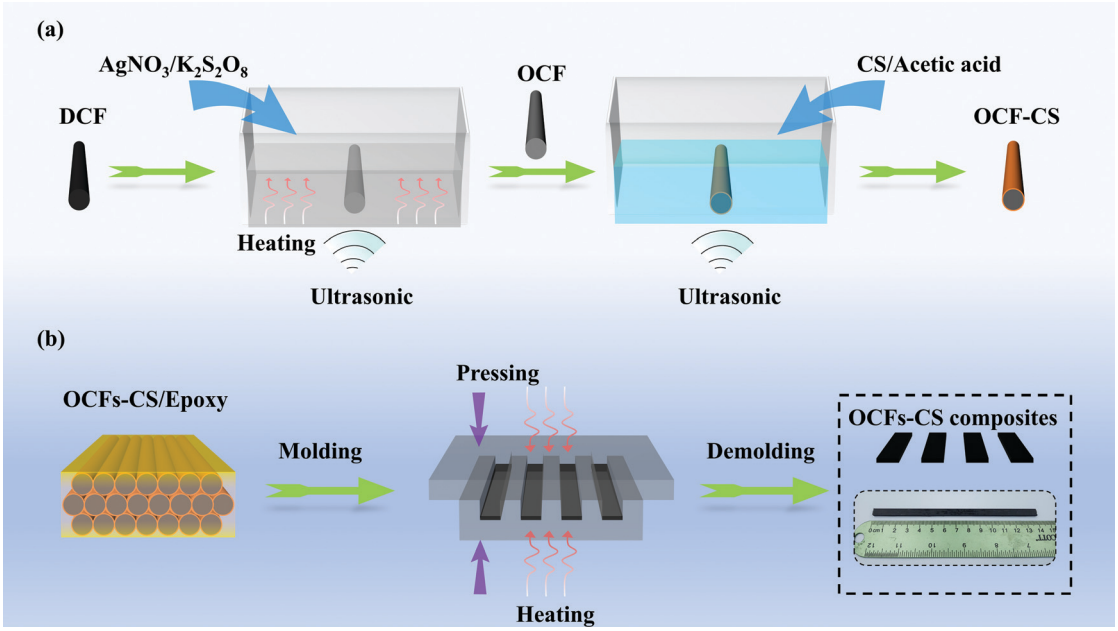

Fig. 1 Schematic figure of (a) CS-encapsulated CFs and (b) OCFs-CS composites.

The surface morphology of the fibers and the fracture surface of the CFRP composites were observed using SEM (JSM-9600, Japan) and TEM (JEM-2100F, Japan). The contact angle between TDE-85 and the CFs was measured using a drop analyzer (DSA25S, Kruss, Germany) to characterize the wettability of the fiber.

According to the ASTM-D3379 standard, a single CF was fixed in the middle of a 20 mm hollow board. The tensile speed was 10 mm s^{-1} until the fiber breaks. The single fiber tensile strength σ_t (GPa) can be calculated from eqn (1):

$$\sigma_t = \frac{F_b}{\pi d^2} \quad (1)$$

where F_b and d (m) are the failure load and the diameter of a single fiber. At least 60 valid data points were tested for each sample.

The interfacial properties of the composites were quantified using an IFSS evaluation system (Beijing Future Material SCI-Tech Co., Ltd, China). The details of the microdroplet debonding test are shown in Fig. 2a. The IFSS (MPa) was calculated using eqn (2):

$$\mathrm{IFSS} = \frac{F_{max}}{\pi d l} \quad (2)$$

where $F_{max}(N)$, $d(m)$, $l(m)$ are the maximum load recorded, the diameter of the fiber embedded in the droplet, and the droplet embedding length, respectively. All the presented results were an average of 50 specimens.

The schematic diagram of the TFBT sample is shown in Fig. 2b. The TFBT tensile strength test was performed using a universal testing machine (Instron 5565, USA). The tensile

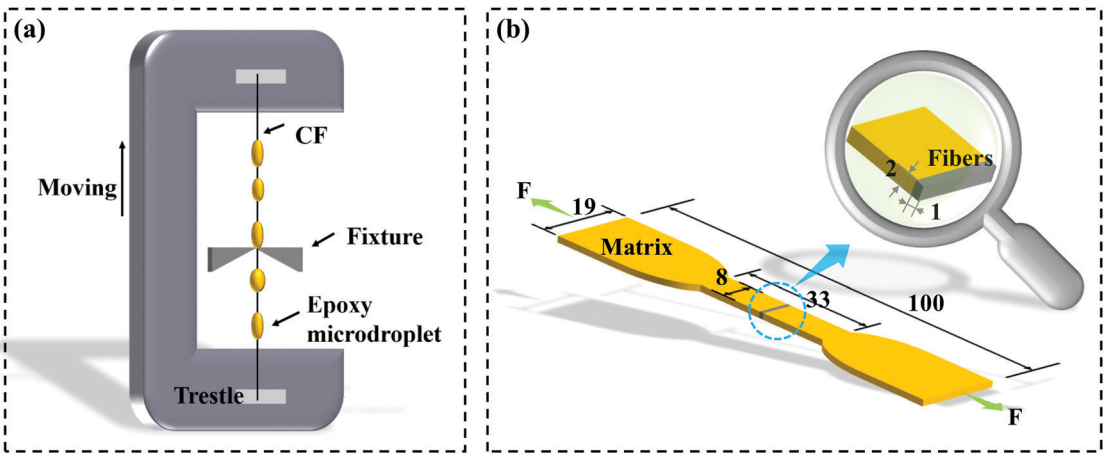

Fig. 2 Schematic diagram: (a) single fiber micro-droplet bonding test and (b) TFBT (in mm).

speed was 1 mm min^{-1}. All results were obtained from the average value of 8 specimens.

According to ASTM D2344, the ILSS of unidirectional CFRP composites was tested using a three-point short-arm bending method. The size of each sample was 20 mm × 6 mm × 2 mm. The ILSS (MPa) was calculated as follows:

$$\mathrm{ILSS} = \frac{3P_{\max}}{4ab} \quad (3)$$

where $P_{\max}$ (N), a (mm), and b (mm) are the maximum value of the load, the width, and thickness, respectively. At least 5 valid data points were tested for each ILSS sample. The longitudinal section and cross-section of the composite after the interlaminar shear test was also observed using SEM.

3 Results and discussion

3.1 Chemical structure of the CF surface

The changes in the structure on the surface of the treated fibers were studied using Raman spectroscopy. As shown in Fig. 3a, there were two peaks at the Raman shifts of 1375 cm^{-1} and 1595 cm^{-1}, which were related to the D and G bands, respectively.[31] The R_I (I_D/I_G) value of the DCFs, OCFs, OCFs-CS1, OCFs-CS2, OCFs-CS3, and OCFs-CS4 was 1.18, 1.20, 1.23, 1.23, 1.25 and 1.30, respectively. The fitting curve of the Raman spectrum is shown in Fig. S3 (ESI†). R_I was related to crystal size and carbon structure and was proportional to the number of defects on the CF surface.[32] For DCFs, the surface was smooth with fewer defects and had the smallest R_I. After oxidation, the surface defects of the fiber increased and the R_I increased slightly. In addition, when the fiber was encapsulated by CS, and the R_I increased with the increase in the CS content. CS increased the degree of fiber disorder.

The change in fiber surface structure is an important factor that causes a change in the surface elements. Thus, the surface elements of the CFs were analyzed using XPS. The percentages of C, N, and O are presented in Fig. 3b. The O element on the surface of the DCFs was derived from the pre-sizing electrochemical oxidation to enhance the surface active sites of the CFs. The O/C ratio increased from 10.6% to 21.8% after the oxidation treatment. Sufficient functional groups for subsequent reactions were provided. The content of O and N increases with the increase in CS content after encapsulation, which was attributed to the abundance of $-NH_2$ and –OH functional groups of CS. The C element content of OCFs-CS1, OCFs-CS2, and OCFs-CS3 decreased with the increase in CS content, while the N and O elements increased gradually. OCFs-CS4 showed the opposite phenomenon. The possible reasons were the high CS content and an uneven distribution on the fiber surface.

The XPS spectrum showed C1s (284.8 eV), N1s (400.5 eV), O1s (532.1 eV), which were the main components of the CFs. Commercial CFs require electrochemical oxidation to increase the active sites of the surface to facilitate sizing. So the surface of DCFs contains a certain amount of the O element. For DCFs and OCFs, the C element can be present as functional groups of C–C, C–O, and O–C═O. After oxidation treatment, the content of the O element increased significantly. The proportion of the O–C═O functional group increased from 7.34% to 9.69%. The results showed that the oxidation system of $AgNO_3/K_2S_2O_8$ mainly increased the content of O–C═O on the surface of the fibers.[29] This provided sufficient functional groups for subsequent reactions.

The percentage of carbon functional groups in the fiber is presented in Fig. 3c, and the peak fitting is presented in Fig. S4

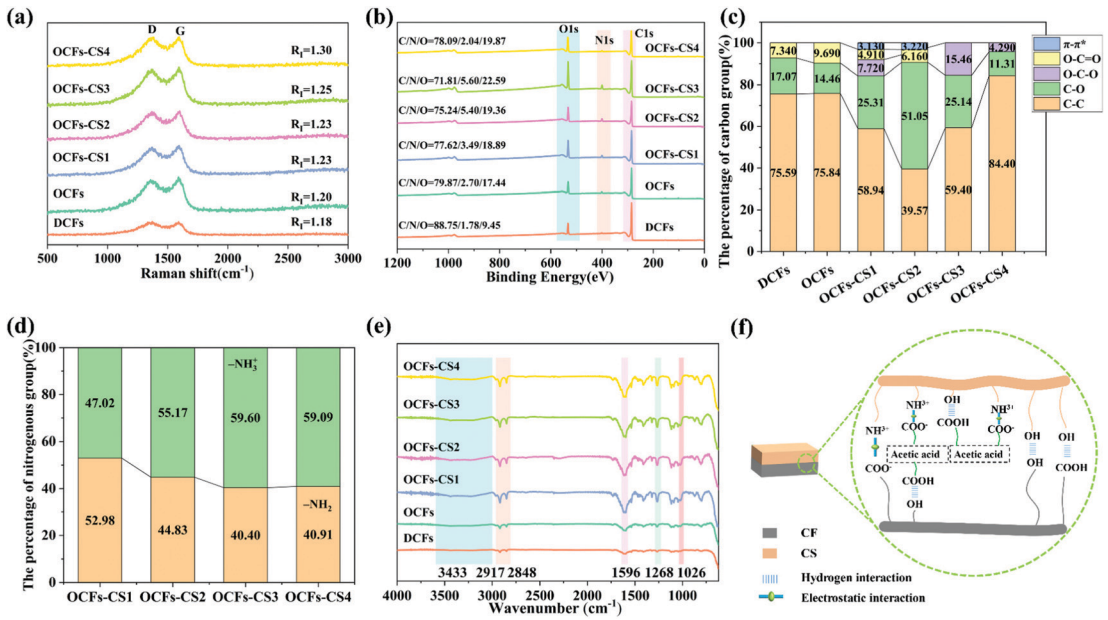

Fig. 3 (a) Raman spectra and R_I of different fibers. (b) Wide-scan XPS spectra. (c) Percentage of carbon groups. (d) Percentage of nitrogenous groups. (e) FT-IR spectroscopy. (f) Schematic diagram of the molecular interactions in CS membrane formation.

(ESI†). For OCFs-CS1, the C element can be classified as C–C (58.94%), C–O (25.31%), O–C–O (7.72%), O–C═O (4.91%) and π–π* (3.13%). This indicated that CS had formed a stable structure on the surface of the fibers.[33] In addition, CS and the CFs were cross-linked *via* π–π* conjugation. When the CS concentration was raised to 0.05 wt% (OCFs-CS2), the ratio of π–π* rose to 3.22%. With the further increase of CS content (OCFs-CS3), the proportion of C–O–C was 15.46%. So far, the content of CS has been very high. For OCFs-CS4, there were mainly C–C (84.40%), C–O (11.31%), and C–O–C (4.29%). Large quantities of CS were encapsulated on the surface of the fiber.

The percentage of N functional groups in the fiber is depicted in Fig. 3d. The peaks were fitted as shown in Fig. S5 (ESI†). The N peaks can be fitted to $-NH_3^+$ near 401.5 eV and $-NH_2$ near 399.5 eV.[34] The percentage of $-NH_3^+$ decreased with the increase in CS content, but the change in $-NH_2$ was the opposite. This can be explained as there being electron transfer between CS and OCF, and $-NH_2$ lost an electron to form positively charged $-NH_3^+$.[28] If the CS content was higher, the bond with the fiber was weaker. In particular, for OCFs-CS3 and OCFs-CS4, the percentage contents of $-NH_3^+$ and $-NH_2$ were almost the same.

The FT-IR spectra of the fibers at different stages are presented in Fig. 3e. The stretching vibrations of the –OH bond were located at 3250 and 3365 cm^{-1}.[35,36] For DCFs and OCFs, there were no apparent absorption peaks at 3250 and 3365 cm^{-1}. After CS encapsulation, the stretching vibration peak of O–H was broadened due to intermolecular hydrogen bonding.[36] The absorption peaks at 2917 cm^{-1} and 2848 cm^{-1} were caused by the stretching vibration of C–H. The absorption bands at 1596 cm^{-1} and 1268 cm^{-1} corresponded to the N–H of amide II and the C–N of amide III, respectively.[24] The strip at 1026 cm^{-1} represented the stretching of the C–O skeleton. The absorption peak was strengthened due to CS encapsulation. Sun *et al.*[37] reported that the –OH group of polyphenols and the –OH or –NH group of CS formed a hydrogen bond, and the hydrogen bond enhanced the interaction between the two compounds. In addition, Liu *et al.*[38] also revealed the interaction between the $-NH_2$ of CS and the –OH or –COOH of protocatechuic acid. Fig. 3f shows a schematic of the interaction between CS and the molecules on the surface of the OCF. The –OH and –COOH in the CFs are connected to –OH in CS through a hydrogen bond interaction. In addition, there was an electrostatic interaction between NH_3^+ and COO^-.[36] Similarly, the –COOH of acetic acid also formed a hydrogen bond with –OH, and there was an electrostatic interaction between NH_3^+ and COO^-.

3.2 Micromorphology and wettability

The influence of CS on the fiber structure was analyzed, and the change in the chemical structure was further verified *via* the microscopic morphology. So, the SEM, TEM, and contact angle images of the CFs are presented in Fig. 4. The surface of the DCFs was smooth and almost free of gullies. After oxidation, the surface of the fiber was etched, and an increase in the roughness can be observed. After CS encapsulation, the surface

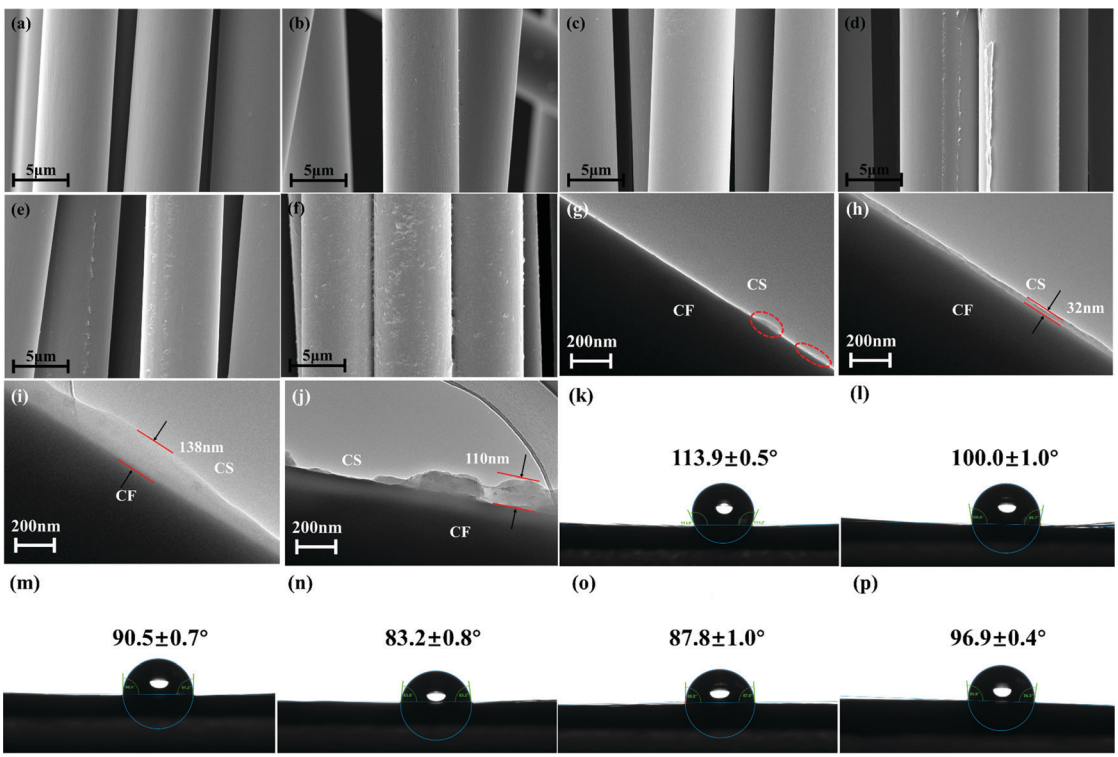

Fig. 4 SEM images of (a) DCFs, (b) OCFs, (c) OCFs-CS1, (d) OCFs-CS2, (e) OCFs-CS3, and (f) OCFs-CS4. TEM images of (g) OCFs-CS1, (h) OCFs-CS2, (i) OCFs-CS3, and (j) OCFs-CS4. Contact angle images of (k) DCFs, (l) OCFs, (m) OCFs-CS1, (n) OCFs-CS2, (o) OCFs-CS3, and (p) OCFs-CS4.

of the OCFs was clearly changed. For OCFs-CS1, there was less CS on the surface of the fiber. It can be seen that CS was distributed sporadically on the surface of the fiber from the TEM image (Fig. 4g). There was not sufficient CS to form a membrane on the fiber surface due to its low content. Most importantly, it can be seen from Fig. 4h (OCFs-CS2) that the membrane covers the fiber surface evenly, with a thickness of about 32 nm. With the increase in CS content, the thickness of the membrane increased gradually. The surface of OCFs-CS3 was wrinkled and the maximum thickness of the membrane was 138 nm (Fig. 4i). However, the thickness of the membrane was not uniform. The thickness of the surface membrane for OCFs-CS4 (Fig. 4j) was 110 nm. Unfortunately, CS tends to aggregate and cannot form a uniform membrane. The surface wrinkles of OCFs-CS4 were larger, and the fiber roughness was also clearly improved.

SEM and TEM confirmed the presence of CS on the surface of the OCFs, and the roughness of the fiber was improved. The surface roughness of the fiber can be characterized by its wettability.[10] The change in contact angle directly characterized the wettability of the CF to epoxy resin, which was the key to the bond between CF and resin. When the liquid touched the fiber, the droplet shape changed and the contact angle decreased due to the adsorption force. The DCFs had a relatively smooth surface and fewer functional groups. The contact angle between the DCFs and TDE-85 was 113.9 ± 0.5°. The surface roughness and the functional group content of the fiber were increased by oxidation, and the contact angle was decreased to 100.0 ± 1°. The contact angles of OCFs-CS1, OCFs-CS2, OCFs-CS3, and OCFs-CS4 were 90.5 ± 0.7°, 83.2 ± 0.8°, 87.8 ± 1.0° and 96.9 ± 0.4° respectively. Because CS was rich in $-NH_2$, –OH, and –COOH groups, the surface roughness of the fiber was improved by the encapsulating process. The surface of the fiber was smooth, and the larger the contact angle, the worse the wettability. The contact angle of the fiber with TDE-85 was further reduced. OCFs-CS2 has the smallest contact angle, which corresponds well with its SEM and TEM images. The results showed that the uniformity of CS encapsulation was the key to affecting the wettability. A uniform CS membrane can be better combined with the resin.

3.3 Single fiber tensile strength tests

The structure and morphology of the fiber were analyzed and observed. In the preparation of the CFs, the surface or core may have various defects (cracks, mechanical damage, holes, *etc.*). CF is a brittle type of material, and the tensile strength of a single fiber is dependent on the number/type of defects. Therefore, the two-parameter Weibull distribution function was selected to analyze the tensile strength. The Weibull distribution of the CFs and the Weibull modulus based on the slope of the fitting curve are presented in Fig. 5a. The fitting of the curve was maintained at 0.98. For the shape parameter (m), DCFs, OCFs, OCFs-CS1, OCFs-CS2, OCFs-CS3, OCFs-CS4 were 4.20, 4.61, 5.19, 4.84, 5.55, and 4.93, respectively.

During the modification process, the structure of the fiber body could easily be damaged. The effect of modification on the fiber can be judged using single fiber tensile strength tests. As shown in Fig. 5b, the tensile strength of a single fiber can directly reflect the change in the strength of the fiber at different treatment stages. The tensile strength of the DCFs and the OCFs was 4.86 GPa and 4.75 GPa. The tensile strength of the OCFs decreased slightly. This was due to the corrosion of $AgNO_3/K_2S_2O_8$ during the oxidation process, which leads to destruction of the surface-ordered structure of the fiber.[29] A large amount of –COOH groups was formed, which destroyed the graphite crystals on the surface of the CF. After CS encapsulation, the tensile strength was improved through the combination of CS with the surface active sites of the fiber. The tensile strength of OCFs-CS1, OCFs-CS2, OCFs-CS3, and OCFs-CS4 were 4.79, 5.07, 5.28, and 4.73 GPa, respectively. Initially, the tensile strength increases with the increase in CS content. However, after a point, the higher the concentration of CS, the lower the tensile strength of a single fiber. Through the single fiber tensile strength tests, it showed that the CS-encapsulated CF

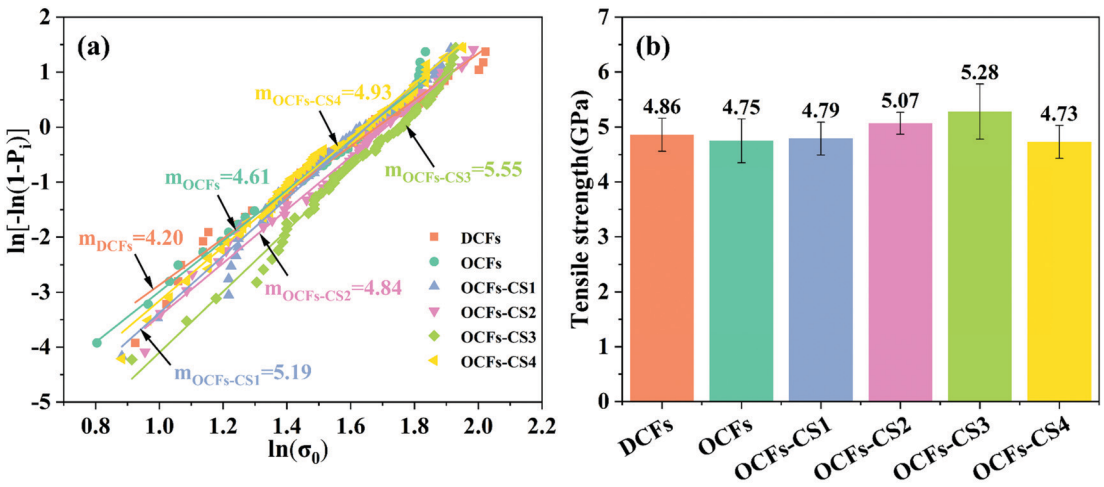

Fig. 5 (a) Weibull distribution curves of different fibers and (b) single fiber tensile strength.

did not damage the structure of the fiber itself. This was an eco-friendly and non-destructive method. Most importantly, the rich functional groups can improve the interfacial properties of the composites.

3.4 Interface properties

The change in the fiber interface characteristics at different stages can be directly characterized using the IFSS, TFBT, and ILSS. The IFSS was analyzed using the micro-drop debonding test. The micro-drop bonding technique has been widely used to characterize the bonding quality of a CF to epoxy.[7] Through the characterization of the poor interface, the interfacial properties of the fibers were further revealed. The SEM images before and after micro-drop debonding are presented in Fig. 6a. The surface of the DCFs was smooth, and the combination of DCFs and epoxy was weak with an IFSS of 39.46 MPa. Oxidation treatment increased the surface activity of the fiber, and the IFSS increased by 25.11% (49.37 MPa). The increase of the specific surface area made the interfacial bonding between the fiber and the matrix stronger. CS improved the interface of the CF by hydrogen bonding and electrostatic interactions. The IFSS of OCFs-CS2 and OCFs-CS3 was 60.63 MPa and 60.11 MPa, respectively, which were 53.65% and 52.33% higher than that of the DCFs. The micro-fracture mechanism was considered to be the visual manifestation of interfacial bond failure.

The droplet bonding technology characterized the bonding ability of a single fiber with epoxy. The TFBT used a bundle of fibers, which was an efficient way to evaluate the bond strength of epoxy.[39] It can better describe the radial change of the fiber. In addition, the TFBT has the advantage that the impregnation process does not require a curing pressure compared with the composite fabrication method. This was a simple and rapid method to evaluate the bonding properties of the fiber/matrix interface.[40] The TFBT specimens before and after tensile fracture are shown in Fig. 6c. After the fracture, the fibers were evenly distributed at both ends of the dumbbell-shaped spline. For DCFs and OCFs, the TFBT tensile strength was 20.09 MPa and 24.46 MPa, respectively. After CS encapsulation, the TFBT tensile strength with different fibers was changed. OCFs-CS2 has the largest TFBT tensile strength (26.95 MPa) with an increase of 34.15%. Compared with OCFs, the TFBT tensile strength of OCFs-CS1 and OCFs-CS3 were slightly reduced, and OCFs-CS4 shows almost no change. According to SEM and TEM, it can be concluded that the uniform membrane structure can improve the interface performance.

The IFSS describes the interface performance between a single fiber and epoxy resin, and the TFBT describes the interface performance between a bundle of fibers and epoxy resin. The difference is that the ILSS reflects the performance of CFRP composites made of many bundles of fibers. The interfacial

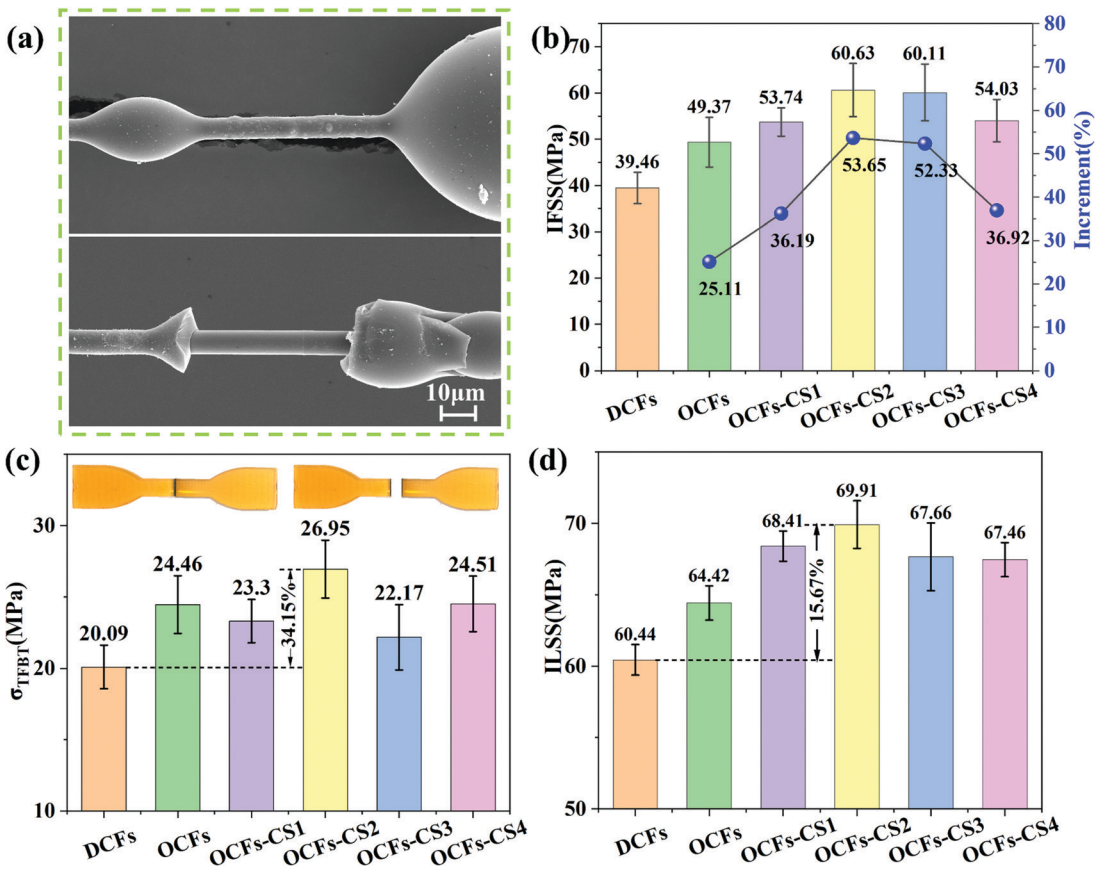

Fig. 6 (a) Micro-droplet SEM pictures of OCFs-CS2 before and after de-bonding. (b) IFSS of the CF/epoxy composites. (c) TFBT specimen of OCFs-CS2 before and after testing, and TFBT of the CF/epoxy composites. (d) ILSS of the CF/epoxy composites.

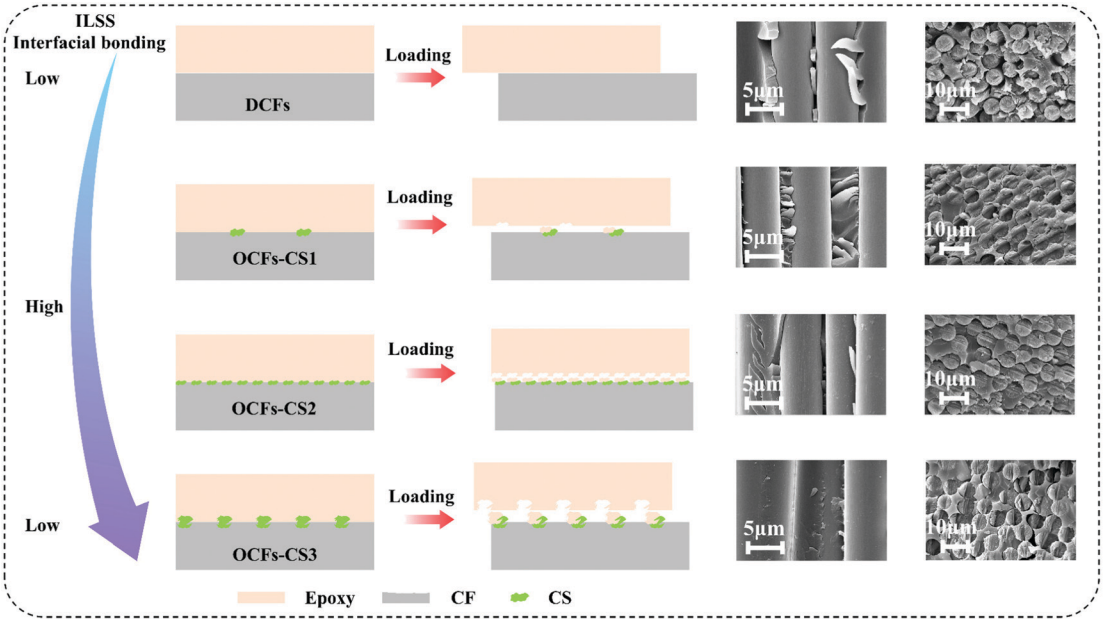

Fig. 7 Failure mode of different CFRP composites.

properties of CS encapsulated CFRP composites were investigated *via* ILSS analysis. As shown in Fig. 6d, the ILSS of DCFs composites was 60.44 MPa. Compared with the DCFs, the ILSS of the OCF composites increased by 6.59%. Oxidation increases the surface active sites of the fiber and improves its binding to epoxy. After CS encapsulation, the corresponding ILSS increased. The ILSS of the OCFs-CS2 composite was 69.91 MPa, an increase of 15.67%. Once again, the excellent membrane structure on the surface of the fiber can improve the interface performance with the epoxy. The ILSS was the strength limit of the composite material under interlaminar shear loading, which can directly evaluate the interlaminar properties of composite materials.[41]

SEM was used to observe the cross-section and longitudinal section of the composites, and the interfacial bonding state and strengthening mechanism of the composites with epoxy resin were studied. Due to the smooth surface of the DCFs, the resin was completely sloughed off from the fiber surface. Furthermore, a portion of the longitudinal section of the fiber was pulled away, leaving more holes and cracks. This showed that the composite has weak interfacial properties. This phenomenon can be correlated with the ILSS data. The interface of the OCFs was improved and the fibers were arranged more closely. The number of holes and cracks was decreased. If the holes and cracks decreased, the fiber and epoxy became closer after CS encapsulation. A certain amount of epoxy remained on the surface of the fiber. The longitudinal section was flatter and has fewer holes and cracks. In particular, OCFs-CS2 has the most resin in the cross-section and is the smoothest in longitudinal section, with almost no holes and cracks.

The interface acts as a transition layer between the CF and the resin matrix. When stress acts on the CFRP composites, the interface can transfer the stress, reduce the stress concentration and reduce the crack formation.[42] The failure mechanism of different composites is presented in Fig. 7. The mechanism of improving the mechanical properties of CF composites was assumed and simulated. For DCF composites, the interface between the DCFs and epoxy was poor. The stress was transferred directly from the resin matrix to the CF, resulting in a crack at the interface and a large slip between the fiber and the matrix. The interface failure of CFRP composites resulted in a decrease in the mechanical properties. For OCF composites, the interfacial adhesion between the fiber and the epoxy matrix was improved due to the increase in active sites on the surface of the OCFs. A small amount of epoxy remained on the surface of the fiber after the shear failure. For OCFs-CS1 composites, the interface performance was further improved. The slip distance between the fiber and the matrix was shortened by the combination of the epoxy and part of the CS after the layer shear failure. For OCFs-CS2 composites, a uniform membrane was formed on the surface of the fiber. When the stress was transferred from the resin matrix to the CF. The interfacial layer can effectively transfer the stress, effectively reducing the interface fracture, thus improving the mechanical properties of the CFRP composites. The corresponding ILSS has the best performance (Fig. 6d). After the shear failure, the epoxy can completely cover the interface layer. There was almost no slip between the fiber and the matrix. For OCFs-CS3 composites, a portion of CS was removed from the epoxy after shear failure. The ILSS performance of the OCFs-CS4 composites was reduced. There were similar failure mechanisms for OCFs-CS4 and OCFs-CS1. This hypothesis can be further verified *via* the SEM and ILSS of the CFRP composites.

4 Conclusion

In this paper, CS was used to encapsulate CFs to improve the interfacial properties of CFRP composites. The optimal test was

carried out by adding different contents of CS (0.025 wt%, 0.05 wt%, 0.075 wt%, and 0.1 wt%). CS formed thin membranes with fibers through hydrogen bonding and electrostatic interactions. A thin membrane of about 32 nm thickness was formed between CS and fiber at the concentration of 0.05 wt%. The surface morphology and wettability of the fiber were greatly improved. According to the results of the single fiber tensile strength test, this method can effectively prevent damage to the CF and improve the tensile strength of a single fiber. Compared with DCF composites, the IFSS, TFBT, and ILSS of OCFs-CS2 composites increased from 39.46 to 60.63 MPa, from 20.09 to 26.95 MPa, and from 60.44 to 69.91 MPa, increases of 53.65%, 34.15%, and 15.67%, respectively. In conclusion, this work provides a certain eco-friendly and non-destructive method for the application of CS in high-performance CFRP composites.

Conflicts of interest

There are no conflicts to declare.

Acknowledgements

The authors thank the Key Science and Technology Plan Project of Zigong City (2021CDZG-12) and the Key R&D projects in Sichuan Province (22ZDYF3323, 22ZDYF3193) for financial support. We also appreciate Hui Wang from the Analytical & Testing Center of Sichuan University for help with SEM characterization. Cheng Zhang thanks the inimitable care and support of Falin Deng over the years.

References

1 A. Pramanik, A. K. Basak, Y. Dong, P. K. Sarker, M. S. Uddin, G. Littlefair, A. R. Dixit and S. Chattopadhyaya, Joining of carbon fibre reinforced polymer (CFRP) composites and aluminium alloys – a review, *Composites, Part A*, 2017, **101**, 1–29.

2 C. Zhang, J. Liu, S. Guo, S. Xiao, Z. Shen and L. Xu, Comparison of microwave and conventional heating methods for oxidative stabilization of polyacrylonitrile fibers at different holding time and heating rate, *Ceram. Int.*, 2018, **44**, 14377–14385.

3 M. C. Paiva, C. A. Bernardo and M. Nardin, Mechanical, surface and interfacial characterisation of pitch and PAN-based carbon fibres, *Carbon*, 2000, **38**, 1323–1337.

4 G. Zhao, J. Liu, L. Xu and S. Guo, Comparative study of conventional and microwave heating of polyacrylonitrile-based fibres, *J. Polym. Eng.*, 2021, **41**, 175–183.

5 X. Zhang, T. Sun, B. Qiu, M. Liang and H. Zou, Investigation on interlaminar behavior of different morphology GO structured carbon fiber reinforced epoxy composites, *Composites, Part B*, 2021, 109492.

6 A. Mirzapour, M. H. Asadollahi, S. Baghshaei and M. Akbari, Effect of nanosilica on the microstructure, thermal properties and bending strength of nanosilica modified carbon fiber/phenolic nanocomposite, *Composites, Part A*, 2014, **63**, 159–167.

7 L. Mei, X. He, Y. Li, R. Wang, C. Wang and Q. Peng, Grafting carbon nanotubes onto carbon fiber by use of dendrimers, *Mater. Lett.*, 2010, **64**, 2505–2508.

8 Q. Peng, Y. Li, X. He, H. Lv, P. Hu, Y. Shang, C. Wang, R. Wang, T. Sritharan and S. Du, Interfacial enhancement of carbon fiber composites by poly(amido amine) functionalization, *Compos. Sci. Technol.*, 2013, **74**, 37–42.

9 Y. Fu, H. Li and W. Cao, Enhancing the interfacial properties of high-modulus carbon fiber reinforced polymer matrix composites via electrochemical surface oxidation and grafting, *Composites, Part A*, 2020, **130**, 105719.

10 T. Sun, M. Li, S. Zhou, M. Liang, Y. Chen and H. Zou, Multi-scale structure construction of carbon fiber surface by electrophoretic deposition and electropolymerization to enhance the interfacial strength of epoxy resin composites, *Appl. Surf. Sci.*, 2020, **499**, 143929.

11 M. Sharma, S. Gao, E. Mäder, H. Sharma, L. Y. Wei and J. Bijwe, Carbon fiber surfaces and composite interphases, *Compos. Sci. Technol.*, 2014, **102**, 35–50.

12 M. A. Montes-Morán, F. W. J. van Hattum, J. P. Nunes, A. Martínez-Alonso, J. M. D. Tascón and C. A. Bernardo, A study of the effect of plasma treatment on the interfacial properties of carbon fibre–thermoplastic composites, *Carbon*, 2005, **43**, 1795–1799.

13 Z. Yao, C. Wang, R. Lu, S. Su, J. Qin, Y. Wang, Z. Ma, H. Wei and Q. Wang, Fracture investigation of functionalized carbon nanotubes-grown carbon fiber fabrics/epoxy composites, *Compos. Sci. Technol.*, 2020, **195**, 108161.

14 Z. Yao, C. Wang, J. Qin, S. Su, Y. Wang, Q. Wang, M. Yu and H. Wei, Interfacial improvement of carbon fiber/epoxy composites using one-step method for grafting carbon nanotubes on the fibers at ultra-low temperatures, *Carbon*, 2020, **164**, 133–142.

15 S. H. Lee, J. Park, J. H. Park, D. M. Lee, A. Lee, S. Y. Moon, S. Y. Lee, H. S. Jeong and S. M. Kim, Deep-injection floating-catalyst chemical vapor deposition to continuously synthesize carbon nanotubes with high aspect ratio and high crystallinity, *Carbon*, 2021, **173**, 901–909.

16 D. Wu, Z. Yao, X. Sun, X. Liu, L. Liu, R. Zhang and C. Wang, Mussel-tailored carbon fiber/carbon nanotubes interface for elevated interfacial properties of carbon fiber/epoxy composites, *Chem. Eng. J.*, 2022, **429**, 132449.

17 L. Ma, N. Li, G. Wu, G. Song, X. Li, P. Han, G. Wang and Y. Huang, Interfacial enhancement of carbon fiber composites by growing TiO_2 nanowires onto amine-based functionalized carbon fiber surface in supercritical water, *Appl. Surf. Sci.*, 2018, **433**, 560–567.

18 Q. Peng, X. He, Y. Li, C. Wang, R. Wang, P. Hu, Y. Yan and T. Sritharan, Chemically and uniformly grafting carbon nanotubes onto carbon fibers by poly(amidoamine) for enhancing interfacial strength in carbon fiber composites, *J. Mater. Chem.*, 2012, **22**, 5928–5931.

19 L. Ma, L. Meng, G. Wu, Y. Wang, M. Zhao, C. Zhang and Y. Huang, Improving the interfacial properties of carbon

fiber-reinforced epoxy composites by grafting of branched polyethyleneimine on carbon fiber surface in supercritical methanol, *Compos. Sci. Technol.*, 2015, **114**, 64–71.

20 J. Lin, P. Xu, L. Wang, Y. Sun, X. Ge, G. Li and X. Yang, Multi-scale interphase construction of self-assembly naphthalenediimide/multi-wall carbon nanotube and enhanced interfacial properties of high-modulus carbon fiber composites, *Compos. Sci. Technol.*, 2019, **184**, 107855.

21 C. Chu, G. Heyi, N. Gu, K. Zhang and C. Jin, Interfacial microstructure and mechanical properties of carbon fiber composite modified with carbon dots, *Compos. Sci. Technol.*, 2019, **184**, 107856.

22 D. Wu, X. Sun, X. Liu, L. Liu and R. Zhang, Simple-effective strategy for surface modification via annealing treatment polydopamine coating, *Appl. Surf. Sci.*, 2021, **567**, 150813.

23 H. Zahra, D. Sawada, C. Guizani, Y. Ma, S. Kumagai, T. Yoshioka, H. Sixta and M. Hummel, Close Packing of Cellulose and Chitosan in Regenerated Cellulose Fibers Improves Carbon Yield and Structural Properties of Respective Carbon Fibers, *Biomacromolecules*, 2020, **21**, 4326–4335.

24 Y. Liu, S. Wang, W. Lan and W. Qin, Fabrication of polylactic acid/carbon nanotubes/chitosan composite fibers by electrospinning for strawberry preservation, *Int. J. Biol. Macromol.*, 2019, **121**, 1329–1336.

25 E. Bilgin Simsek, D. Saloglu, N. Ozcan, I. Novak and D. Berek, Carbon fiber embedded chitosan/PVA composites for decontamination of endocrine disruptor bisphenol-A from water, *J. Taiwan Inst. Chem. Eng.*, 2017, **70**, 291–301.

26 C. Tang, D. Hu, Q. Cao, W. Yan and B. Xing, Silver nanoparticles-loaded activated carbon fibers using chitosan as binding agent: preparation, mechanism, and their antibacterial activity, *Appl. Surf. Sci.*, 2017, **394**, 457–465.

27 S. Davarpanah, N. M. Mahmoodi, M. Arami, H. Bahrami and F. Mazaheri, Environmentally friendly surface modification of silk fiber: Chitosan grafting and dyeing, *Appl. Surf. Sci.*, 2009, **255**, 4171–4176.

28 H. Li and L. Peng, Antimicrobial and antioxidant surface modification of cellulose fibers using layer-by-layer deposition of chitosan and lignosulfonates, *Carbohydr. Polym.*, 2015, **124**, 35–42.

29 J. Yu, L. Meng, D. Fan, C. Zhang, F. Yu and Y. Huang, The oxidation of carbon fibers through $K_2S_2O_8/AgNO_3$ system that preserves fiber tensile strength, *Composites, Part B*, 2014, **60**, 261–267.

30 C. Zhang, X. Zhang, Y. Luo, M. Liang and H. Zou, Green and Nondestructive Method for Constructing Multiscale Carbon Fiber Reinforcement *via* Encapsulating Chitosan and Grafting Carbon Nanotubes, *ACS Appl. Nano Mater.*, 2021, **4**, 13388–13397.

31 A. Jorio and R. Saito, Raman spectroscopy for carbon nanotube applications, *J. Appl. Phys.*, 2021, **129**, 021102.

32 M. S. A. Rahaman, A. F. Ismail and A. Mustafa, A review of heat treatment on polyacrylonitrile fiber, *Polym. Degrad. Stab.*, 2007, **92**, 1421–1432.

33 M. Zhang, L. Jin, Y. Zhai, C. Cheng, F. Yan, Y. Liu, L. Liu and Y. Ao, Bio-inspired gallic acid-gelatin coating: A novel strategy for eco-friendly interfacial modification of carbon fiber composites, *Compos. Commun.*, 2021, **26**, 100790.

34 Y. M. Nikolenko, V. G. Kuryavyi, I. V. Sheveleva, L. A. Zemskova and V. I. Sergienko, Atomic force microscopy and X-ray photoelectron spectroscopy study of chitosan–carbon fiber materials, *Inorg. Mater.*, 2010, **46**, 221–225.

35 C. Li and J. Li, Preparation of chitosan–ferulic acid conjugate: structure characterization and in the application of pharmaceuticals, *Int. J. Biol. Macromol.*, 2017, **105**, 1539–1543.

36 K. Li, J. Zhu, G. Guan and H. Wu, Preparation of chitosan–sodium alginate films through layer-by-layer assembly and ferulic acid crosslinking: film properties, characterization, and formation mechanism, *Int. J. Biol. Macromol.*, 2019, **122**, 485–492.

37 L. Sun, J. Sun, L. Chen, P. Niu, X. Yang and Y. Guo, Preparation and characterization of chitosan film incorporated with thinned young apple polyphenols as an active packaging material, *Carbohydr. Polym.*, 2017, **163**, 81–91.

38 J. Liu, S. Liu, Q. Wu, Y. Gu, J. Kan and C. Jin, Effect of protocatechuic acid incorporation on the physical, mechanical, structural and antioxidant properties of chitosan film, *Food Hydrocolloids*, 2017, **73**, 90–100.

39 G. Qi, B. Zhang and Y. Yu, Research on carbon fiber/epoxy interfacial bonding characterization of transverse fiber bundle composites fabricated by different preparation processes: Effect of fiber volume fraction, *Polym. Test.*, 2016, **52**, 150–156.

40 S. Deng, B. Qi, M. Hou, L. Ye and K. Magniez, Assessment of interfacial bonding between polymer threads and epoxy resin by transverse fibre bundle (TFB) tests, *Composites, Part A*, 2009, **40**, 1698–1707.

41 B. Qiu, T. Sun, M. Li, Y. Chen, S. Zhou, M. Liang and H. Zou, High micromechanical interlocking graphene oxide/carboxymethyl cellulose composite architectures for enhancing the interface adhesion between carbon fiber and epoxy, *Composites, Part A*, 2020, **139**, 106092.

42 X. Yuan, B. Zhu, X. Cai, J. Liu, K. Qiao and J. Yu, Optimization of interfacial properties of carbon fiber/epoxy composites *via* a modified polyacrylate emulsion sizing, *Appl. Surf. Sci.*, 2017, **401**, 414–423.

